



IJRASET

International Journal For Research in
Applied Science and Engineering Technology



INTERNATIONAL JOURNAL FOR RESEARCH

IN APPLIED SCIENCE & ENGINEERING TECHNOLOGY

Volume: 10 Issue: V Month of publication: May 2022

DOI: <https://doi.org/10.22214/ijraset.2022.42182>

www.ijraset.com

Call:  08813907089

E-mail ID: ijraset@gmail.com

A Memory Based Current Algorithm for Pole-to-Pole Fault Detection in Microgrids

Nirupama P Srinivas¹, Sangeeta Modi²

^{1,2}Department of Electrical and Electronics Engineering, PES University, Bangalore, India

Abstract: *The world's growing attention to sustainable energy and development can be causal to the recently observed disrupt in the existing global power system networks. Moreover, an additional incentive towards this change are the challenges associated with the traditional power grid, including its rigid structure, aging architecture, and ecologically profligate nature. Modern power systems have observed a rapidly growing trend of decentralized energy generation in the recent past. A prominent structure incorporating decentralized energy generation and renewable energy are microgrids. While microgrids promote on-site generation and distributed energy resources (DERs), their unique characteristics of bidirectional flow of power, renewable generational intermittency, and varying levels of current causes challenges uncommon to the traditional grid. One of the vital challenges associated with microgrids is the protection of microgrids against faults and disturbances that can cause impairment to life and property. Conventional protection algorithms are ineffective in protecting the system from faults due to the unconventional topology of the microgrid. This paper attempts to contribute to work in the sector related to the protection of microgrids. This paper presents the pole-to-pole fault analysis of a hybrid photovoltaic system and presents a current based algorithm for the detection of DC pole-to-pole faults in the system under study. The protection algorithm is further verified on a hybrid Photovoltaic-Wind-Battery microgrid.*

Keywords: *DC Faults, Hybrid Microgrids, Power Systems, Protection Algorithm, DERs*

I. INTRODUCTION

Over the last few years, renewable energy sources, including wind energy and solar energy, have observed a rise in interest due to sustainable energy goals. The onset of rapid technological advances in renewable energy has led to a disrupt in existing power system structures. One of the most prominent changes is the development of distributed generation. While conventional power systems follow a strict top-down topology with a unidirectional flow of power, distribution generation allows renewable integration to an existing power network, offering bidirectional flow of power, and endorsing a peer to peer power network topology. Another important consequence of the recent strides in energy generation are autonomous power systems, or microgrids. Microgrids are self-sufficient distributed energy systems which serve a clearly defined geographic footprint with control capability. Further, they are capable of disconnection from the traditional grid, operating autonomously.

Microgrids are breakthrough is promoting renewable energy, due to their unique provision of distributed generation. Microgrids aim to promote a high amount of renewable incorporation in the system. The exclusive characteristics of microgrids causes challenges related to power quality, protection from faults and disturbances, resynchronization with the main grid, and more. [1]

DC microgrids offer advantages of improved power quality, higher efficiency due to reduced transmission losses and reduced conversion stages used for DC loads. However, the major obstacle to DC microgrids is the immature protection system, high initial cost, and the general lack of guidelines and standards as compared to AC systems.

While numerous researchers around the world have focused on protection in AC systems, protection in DC systems remains to be challenging and relatively unexplored. Moreover, the lack of zero crossing in voltage and current values make the DC protection challenge tough to solve. This paper suggests a memory-based defence algorithm for an LVDC microgrid based on current. The system under study is a solar based hybrid microgrid with three DC loads and three AC loads. In this study, the system operates autonomously from the main power grid, i.e., the point of common coupling (PCC) between the grid and the network is kept open. The work presented is implemented for the DC side of the microgrid. The algorithm helps in the detection of pole-to-pole faults in the system under consideration. This paper can be explored in 5 segments. The first section encompasses of the literature review of microgrids, microgrid challenges, DC faults, and existing protection algorithms. The second segment introduces the network under study and presents the pole-to-pole fault study of the system. The following section presents the current algorithm, and the analysis of its results on the system under study. The fourth section concludes with the results, followed by the conclusion and future work to be carried out.

II. LITERATURE REVIEW

This section presents literature review on microgrids, challenges associated with microgrids, faults in power systems, and existing power system protection algorithms.

A. Microgrids

Microgrids can be defined as the decentralized synchronous operation of electrical loads, energy store systems (ESS), and Distributed energy resources (DERs) to provide reliable, secure, and consistent power to its consumers. [2] Microgrids can competently integrate distributed generation and provide pathways for large scale development of renewable energy and can efficiently solve the global electrification challenge. [3]

Microgrids appear as a single entity as per the traditional power grid and are a powerful integration of energy reserves, energy storage, and loads. Microgrids are linked to their host power system, or the traditional power grid, through a switching mechanism, commonly known as the point of common coupling. [4]

Microgrids, based on their power are classified into AC microgrids, DC microgrids, and hybrid microgrids. [5] In an AC microgrid, all resources, loads, and storage units are connected to a common AC bus. AC microgrids encompass of many dispersed generational elements. DC microgrids are interfaced through a DC system, where the voltage of operational is roughly 300-600V. [6] Hybrid microgrids comprise of various parallelly interlinked distributed generational units with controlled topologies. Hybrid microgrids offer superiority over AC or DC microgrids by offering the option to reduce multiple intermediate conversion stages, thus increasing overall efficiency. DC systems consist of several Distributed Energy Resources (DERs) structures which involve photovoltaic, fuel cells and energy storage, and electrical loads, including EVs, Light Emitting Diodes (LEDs) which are powered by DC sources. DC networks have an added benefit in power quality which influences the utility grid. DC microgrids have a opportune apparatus for incorporating DERs with local loads into a completely cohesive network.

B. Challenges Associated with Microgrids

While microgrids provide unmatched advantages of higher efficiency, last mile connectivity, reduced transmission losses, autonomous operation and easy integration of renewable resources, their characteristic of bidirectional power flow, integration of intermittent renewable energy resources, and energy storage components cause issues related to power quality, resynchronization, inertia, islanding, and protection. A challenge popular amongst researchers worldwide is the microgrid protection challenge. [7]

Developing a robust protection scheme for microgrids proves to be perplexing due to the bidirectional flow of power, and inherent intermittency of renewable energy resources causing varying dynamics in fault currents. The latter reason also causes the irksome issue of blinding of protection, and sympathetic tripping. Blinding of protection refers to the controller's obliviousness to detecting a fault in the system due to reduced contribution from sources, and failure to recognize uncharacteristic current. Sympathetic or nuisance tripping can be defined as the operation of a protective element in an unfaulted section or portion of the microgrid due to the presence of fault in another portion of the network. Nuisance tripping in microgrids with renewable resources can also occur due to a sudden change in irradiation, in the case of solar energy, or a sudden change in wind speed, as for wind energy.

The main causes for the microgrid challenge of protection are

- 1) *Variation in fault current level:* This is usually due to the intermittency of DERs, which are mostly renewable in nature, and reduced contribution from the main grid due to islanding.
- 2) *Discrimination of Different Devices:* The fault current is altered in the case of DGs connected at a longer distance leading to increase in the impedances. This decreases the fault current and thereby affecting the operation of the relays because the relay discrimination is influenced by the magnitude of the fault current. Again, this discrimination varies with the situation depending upon the mode of operation of microgrid as isolated and grid integration case. In case of islanded mode, the fault current is lowered as a result may lead non-operation of the relays. Hence, the conventional scheme of protection must be updated as per the current situation for effective operation and control of the power system. [8]
- 3) *Reduced Influence of the Impedance Relays:* The influence is an important parameter for the operation of the relay that depends upon the distance between the fault and relay locations. The fault current is reduced with the above distance thereby affecting the operation of the relay. [9]
- 4) *Reverse Power Flow:* As the sources are integrated from both the ends, the power and hence the current flow from both the directions creating an ambiguity in the operating conditions of the conventional relays. The inverter based DGs also inject lots of harmonics and affect the relay operating parameters such as current, voltage and frequency. Hence, the protection system in microgrid must be designed to overcome the effects of the reverse power flows because of the presence of DGs

- 5) *Islanding*: Islanding is a phenomenon and occurs when DG/microgrid operating in grid-connected mode gets isolated due to some faults/abnormal conditions but continues to supply the local loads. Under the islanding condition the system parameters at PCC are greatly affected leading to mis-operation of the protective relays.

C. Faults in Power Systems

Faults in power systems are unfavourable disturbances that disrupt the normal operation of the power system and can potentially cause severe damage to life and property. Faults in power systems cause high current surges, low voltage, reversed power flow and unbalance of phases in AC systems. Faults are usually caused due to lightning strikes, heavy rains, accumulation of weight on transmission lines, and aging architecture. Faults are primarily categorized into open circuit (OC) faults and short circuit (SC) faults. DC faults are usually classified into pole-to-pole faults (short circuit faults) and pole-to-ground faults (open circuit faults). [12]

In the DC systems, faults occur as pole-to-pole (PP) and pole-to-ground (PG) faults. In PG faults, one or both conductors are connected to the ground [13]. Hence, PG faults are of high impedance. In pole-to-pole faults, the conductors are directly coupled to each other. Hence, pole-to-pole faults are of low-impedance, and these faults are more noticeable and hazardous. [14]

Due to the absence of a frequency component and zero-crossing, DC faults are accompanied with unique challenges [15]. A few of the tasks related with DC faults are the requirement of high speed to clear faults, identifying the faulted location in the loop, and communication time delay in HVDC lines [16]. These challenges are attributed to the track of fault current, synchronization problems of current-based relay, unsuitability of AC circuit breakers (CBs), variation in the SC levels, and low fault current capability of inverters [17-19]. Fig. 1 represents the stages of short circuit current during a DC fault.

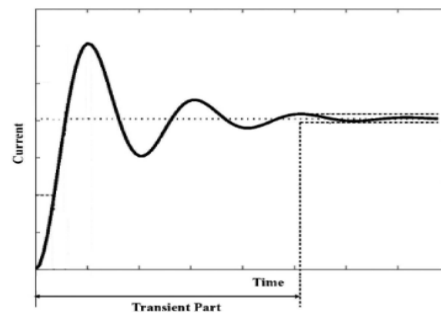


Fig. 1: SC Current during a DC Fault

D. Protection in Power Systems

To ensure stable supply or reliable power to consumers connected to any power network, it is important to design a robust protection scheme. While a single protection scheme cannot be marked ideal for all systems, one must make an optimization of various parameters while approximating the strength of a protection scheme. [10] Few of the factors while selecting a protection scheme include reliability, selectivity, sensitivity, and speed.

One of the most popular algorithms for protection of power systems is the overcurrent algorithm. [11] This is since a primary consequence of a fault is a surge of current, normally much higher than nominal current levels. The overcurrent algorithm is used in power systems to inhibit elements from extracting an unwarranted amount of current, which results in severe damage. The relays used in this algorithm usually are of two types: directional and non-directional. Other popular algorithms include voltage-based algorithm, impedance-based algorithm, differential protection, and distance-based protection.

III. SYSTEM UNDER CONSIDERATION

The system under study is a hybrid radial system. On the DC Side, there are two photovoltaic arrays and three load centres of constant demand associated to a common bus. The common bus is coupled to a bidirectional converter, which is the connecting point of the DC and AC side of the microgrid. The AC side of the microgrid has three load centres of constant demand connected through an AC Filter and is interfaced to the utility grid. In this study, the PCC or the point of common coupling to the utility grid is open, thus resultant in the microgrid functioning in an islanded mode. The solar panels supply 100.72kW under optimal conditions. The total load demand is 100kW. The system under consideration is divided into 6 zones for ease of study and analysis. The system is simulated through MATLAB and Simulink. Fig. 2 represents the block diagram of the microgrid under study with the discretization of zones.

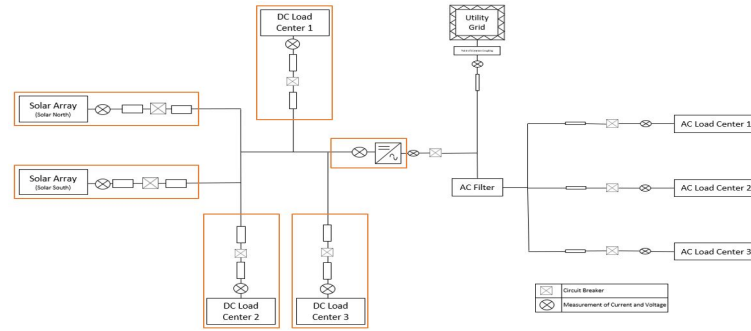


Fig. 2: Block Diagram of System Under Consideration

A. System Under Normal Conditions

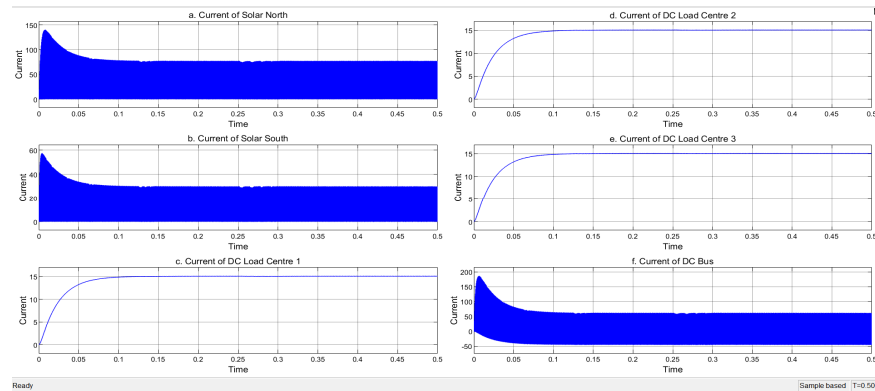


Fig. 3: Current of the System Under Normal Conditions

Fig. 3 represents the current of various zones of the network under normal settings. Fig. 3.a. represents the current of the north side solar array. The peak during the transient stage is almost 140A, followed by steady state value of around 75A. The current of the south side solar array, displayed in Fig. 3.b., has a transient peak of around 58A, followed by stabilization at 30A. Fig. 3.c., Fig. 3.d., and Fig. 3.e. represent the current waveforms near Load Centre 1, Load Centre 2, and Load Centre 3. All three show similar values with steady state drawing approximately 15A of current. Fig. 3.f. is the current of the common bus before the inverter. With a transient peak of around 180A, the current stabilizes close to 60A.

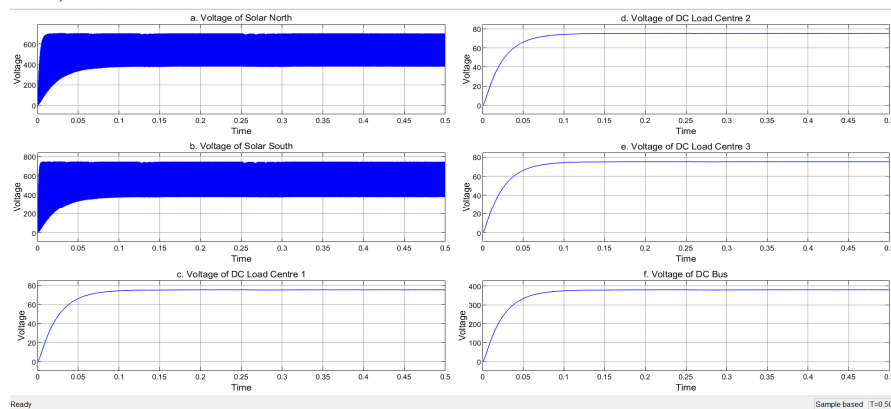


Fig. 4: Voltage of the System Under Normal Conditions

The voltage of various zones under normal conditions in the system is displayed in Fig. 4. Fig. 4.a. represents the voltage waveform of the north solar zone, and the steady state voltage of the zone is around 650V. The south side solar zone's voltage under normal simulation conditions is represented by Fig. 4.b. 640V is the approximate steady state value of the zone. Fig. 4.c. represents the voltage near to the Load Centre 1, where the steady state voltage is around 75V. Fig. 4.d. and Fig. 4.e. show similar results with each load drawing around 75A. the voltage of the common DC bus is approximately 380V, as shown in Fig. 4.f.

B. Fault in the Solar North Zone

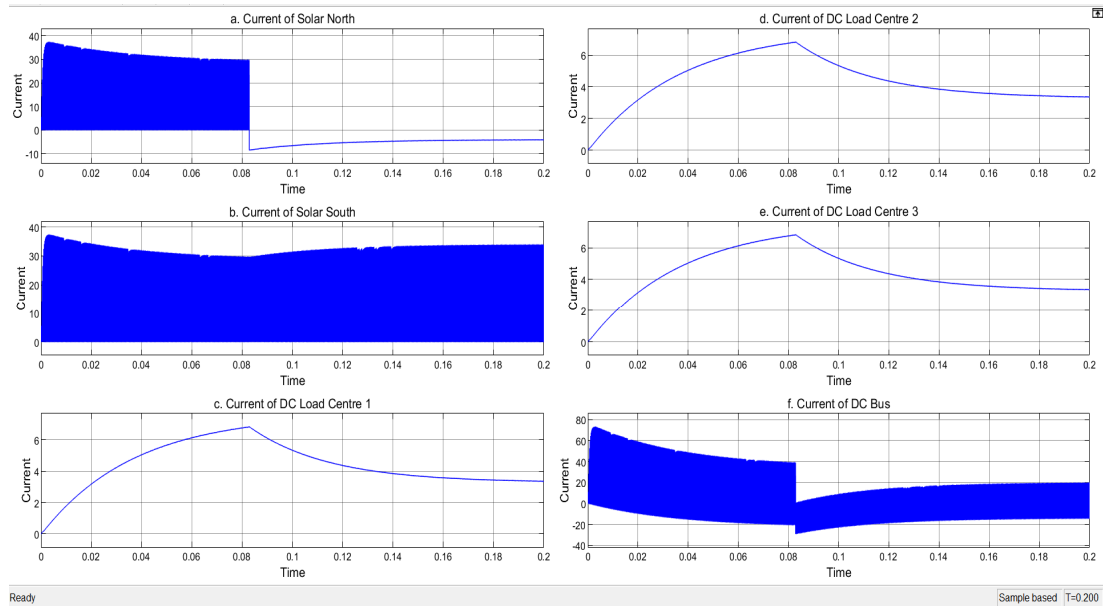


Fig. 5: Current during a Pole-to-Pole Fault in the Solar North Zone

The current change when a pole-to-pole fault has been created in the solar north zone is displayed in figure. Fig. 5.a. represents the current change in the faulted zone, which shows a drop from 30A to around -10A followed by stabilization at approximately -5A. when the fault has been created in the solar north zone, change is observed in the current flowing near to the solar south zone, as displayed in Fig. 5.b. the current of this zone follows a sudden increase by almost increase by about 4-5A. as in Fig. 5.c., Fig. 5.d., and Fig. 5.e., the DC loads are affected by a current decrease by about 3A. The effect of the pole-to-pole fault in the solar north zone is evident in the common DC bus, through Fig. 5.f. the current decreases sharply from 40A under normal conditions to almost 3A, stabilizing at approximately 20A.

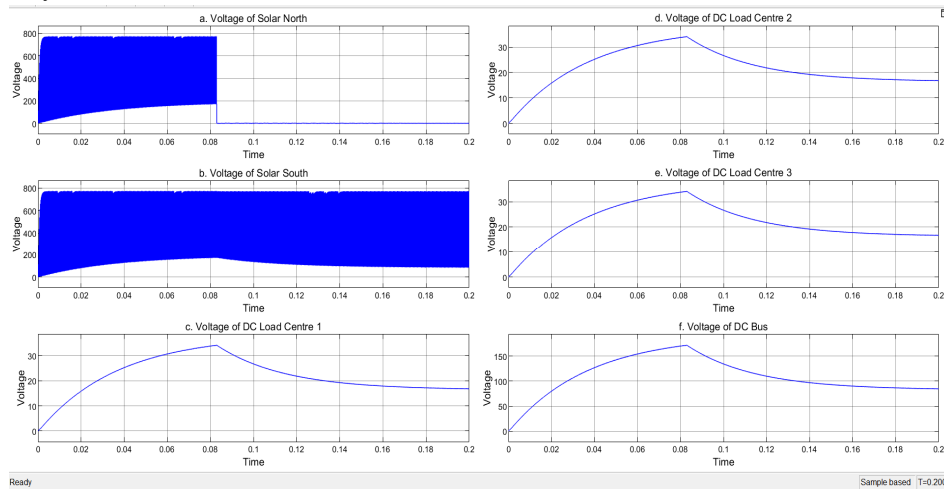


Fig. 6: Voltage during a Pole-to-Pole Fault in the Solar North Zone

When a pole-to-pole fault is created near the North Solar zone, the voltage change is displayed in Figure. the voltage of the solar north zone, where the fault has been created, shows a sharp drop from steady state value to 0V, as shown in Fig. 6.a. Fig. 6.b. represents the voltage change in the south solar zone under the same conditions. There is observed change of the minimum and maximum transient values when the fault has been created. All the DC Loads show significant voltage drop to a steady state of about 15V, as shown in Fig. 6.c., Fig. 6.d., and Fig. 6.e. The DC bus voltage is affected, as displayed in Fig. 6.f., where the voltage drops by around 80V, from a steady state value of almost 160V, to around 75V.

C. Fault in the Solar South Zone

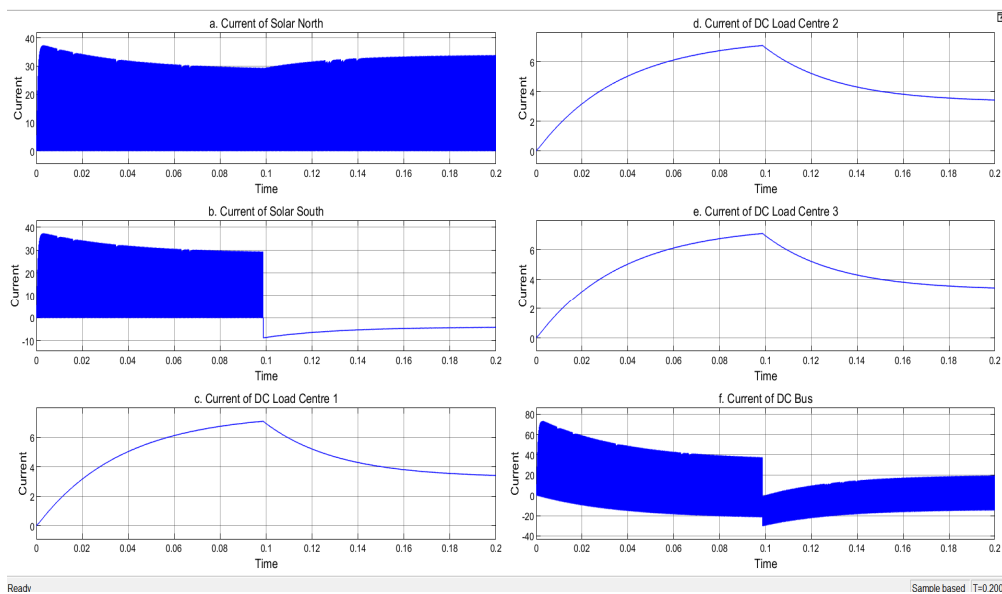


Fig. 7: Current during a Pole-to-Pole Fault in the Solar South Zone

The current change when a pole-to-pole fault has been created in the solar south zone is displayed in figure. Fig. 7.a. represents the current change in the solar north zone, which shows a mild increase in current. when the fault has been created in the solar south zone, change is observed in the current as displayed in Fig. 7.b. the current of this zone follows a sudden decrease to around -10A followed by a stable value to approximately -5A. as in Fig. 7.c., Fig. 7.d., and Fig. 7.e., the DC loads are affected by a current decrease by about 3A. The effect of the pole-to-pole fault in the solar north zone is evident in the common DC bus, through Fig. 7.f. the current decreases sharply from 40A under normal conditions to almost 3A, stabilizing at approximately 20A.

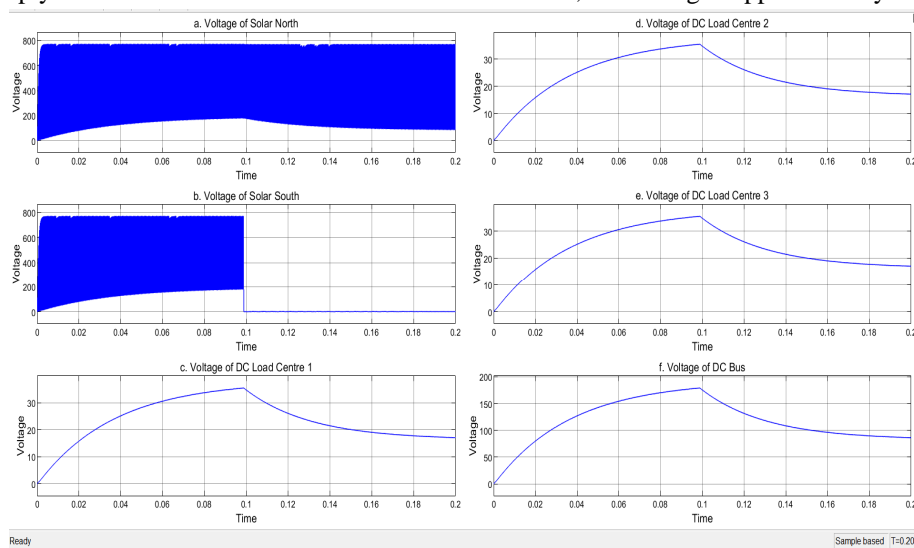


Fig. 8: Voltage during a Pole-to-Pole fault in the Solar South Zone

When a pole-to-pole fault is created near the South Solar zone, the voltage change is displayed in Fig. 8. the voltage of the solar north zone shows a change in transients, as shown in Fig. 8.a. Fig. 8.b. represents the voltage change in the south solar zone where the fault has been created. There is a sharp drop from steady state value to 0V. All the DC Loads show significant voltage drop to a steady state of about 15V, as shown in Fig. 8.c., Fig 8.d., and Fig. 8.e. The DC bus voltage is affected, as displayed in Fig. 8.f., where the voltage drops by around 80V, from a steady state value of almost 160V, to around 75V.

D. Fault in the DC Load Centre 1

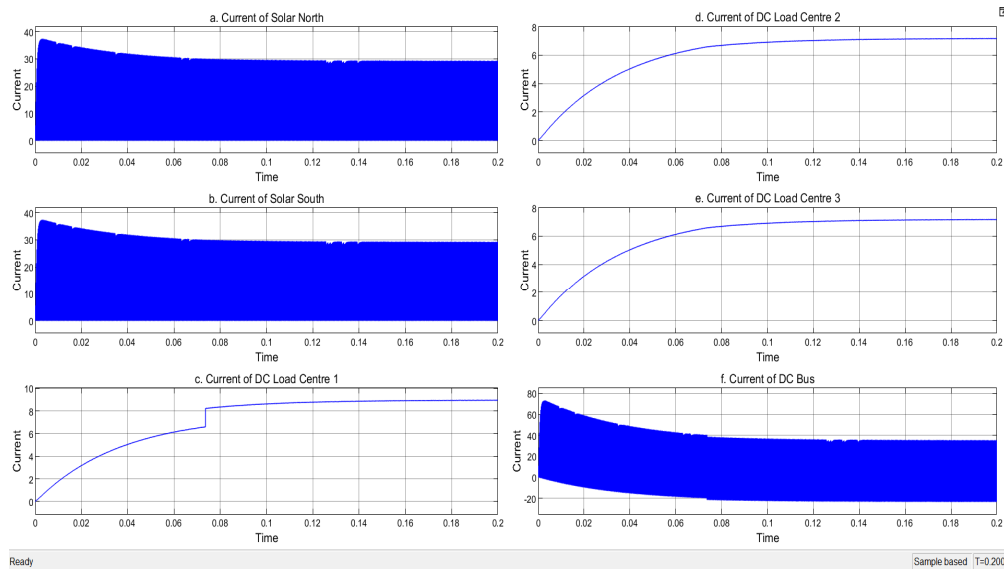


Fig. 9: Current during a Pole-to-Pole Fault in the DC Load Centre 1

When a pole-to-pole fault is created near the solar north zone, the current is graphically represented in figure. while the current through the solar north and south side remain unchanged, as represented in Fig. 9.a. and Fig. 9.b. Fig. 9.c. represents the current through DC Load Centre 1 and shows an increase of approximately 3A. similarly, the DC bus shows a decrease of around 3A when the fault is created, as per Fig. 9.f. Fig. 9.d. and Fig. 9.e. represent the current through DC Load Centre 2 and DC Load Centre 3 and they show no significant change.

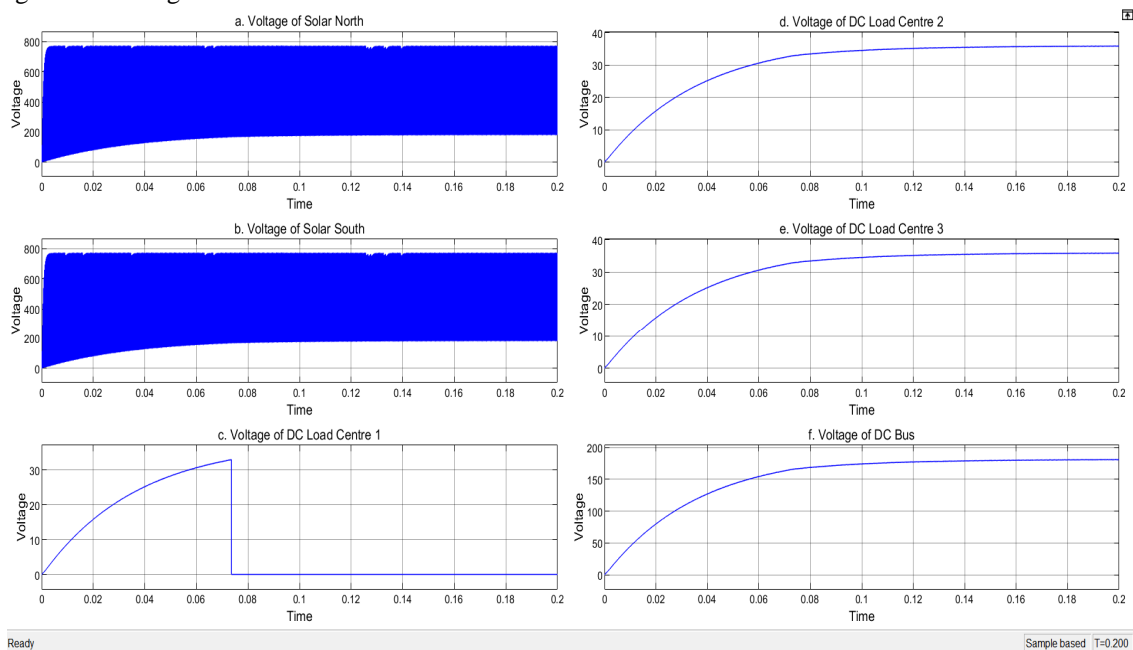


Fig. 10: Voltage during Pole-to-Pole Fault near DC Load Centre 1

The voltage change through various zones in the system is represented by figure. Fig. 10.a. represents the voltage readings in the solar north zone while Fig. 10.b. represents the voltage readings in the solar south zone. Both show no significant change. The faulted zone's voltage readings are represented by Fig. 10.c., where is an observed decrease of voltage from 33V to 0V. the voltage of the DC Load Centre 2 (Fig. 10.d) and DC Load Centre 3 (Fig. 10.e.) show no significant change, like the voltage across the DC Bus, represented by Fig. 10.f.

E. Fault near the DC Load Centre 2

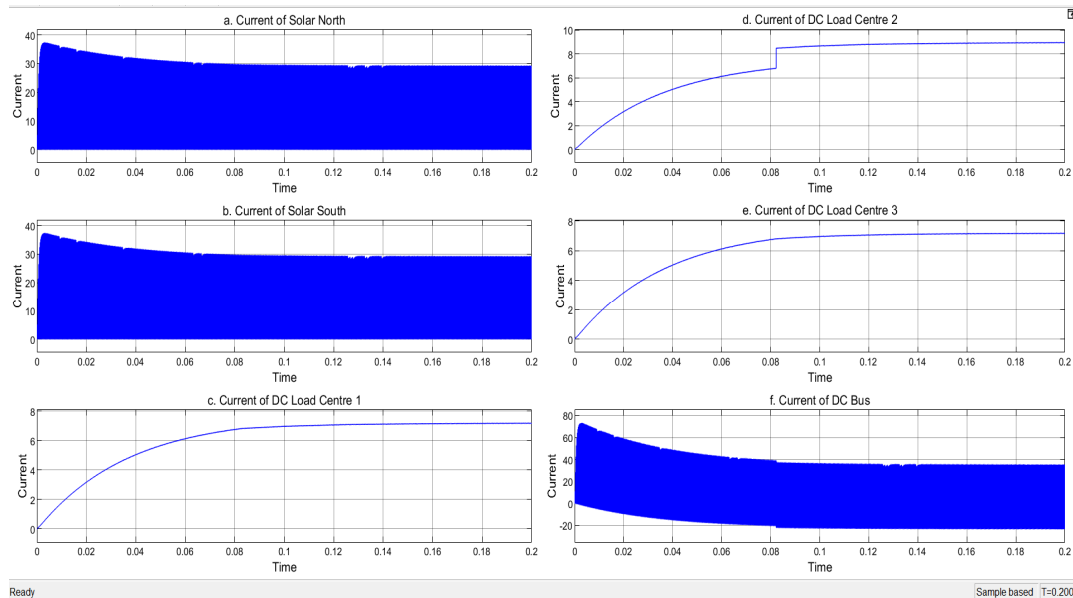


Fig. 11: Current during a Pole-to-Pole Fault near the DC Load Centre 2

Fig. 11 represents the current of various zones of the system when a fault is created near the DC Load Centre 2. Fig. 11.a. represents the current through solar north zone and Fig. 11.b. represents the current through the south zone when the pole-to-pole fault has been created. It is implied that no significant change has been observed in these two zones. Fig. 11.c. and Fig. 11.e. represent the current change in DC Load Centre 1 and DC Load Centre 3. There is no significant change observed in these two zones. However, the current through the DC bus, as shown in Fig. 11.f. shows a sudden decline of around 4A. Fig. 11.d. represents the current through Load Centre 2. The current is affected by a sharp drop from steady state current of 7A to 9A.

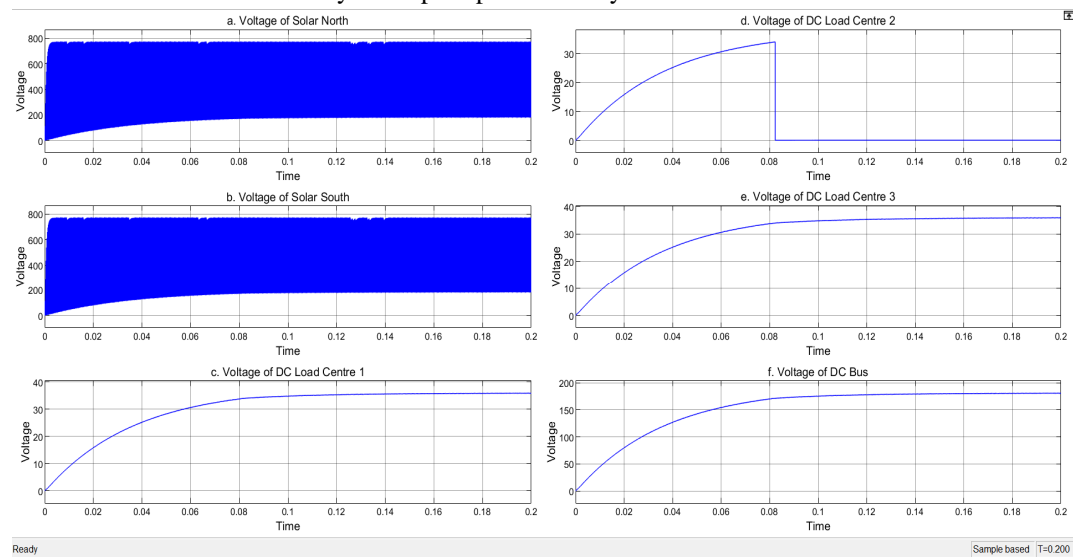


Fig. 12: Voltage during a Pole-to-Pole fault near the DC Load Centre 2

Fig. 12 represents the voltage of various zones of the system when a fault is created near the DC Load Centre 2. Fig. 12.a. represents the voltage through solar north zone and Fig. 12.b. represents the voltage through the south zone when the pole-to-pole fault has been created. It is implied that no significant change has been observed in these two zones. Fig. 12.c. and Fig. 12.e. represent the voltage change in DC Load Centre 1 and DC Load Centre 3. There is no significant change observed in these two zones, as well as the voltage through the DC bus, as displayed in Fig. 12.f. Fig. 12.d. represents the voltage through Load Centre 2. The voltage is affected by a sharp drop from steady state voltage of 33V to 0V.

F. Fault near the DC Load Centre 3

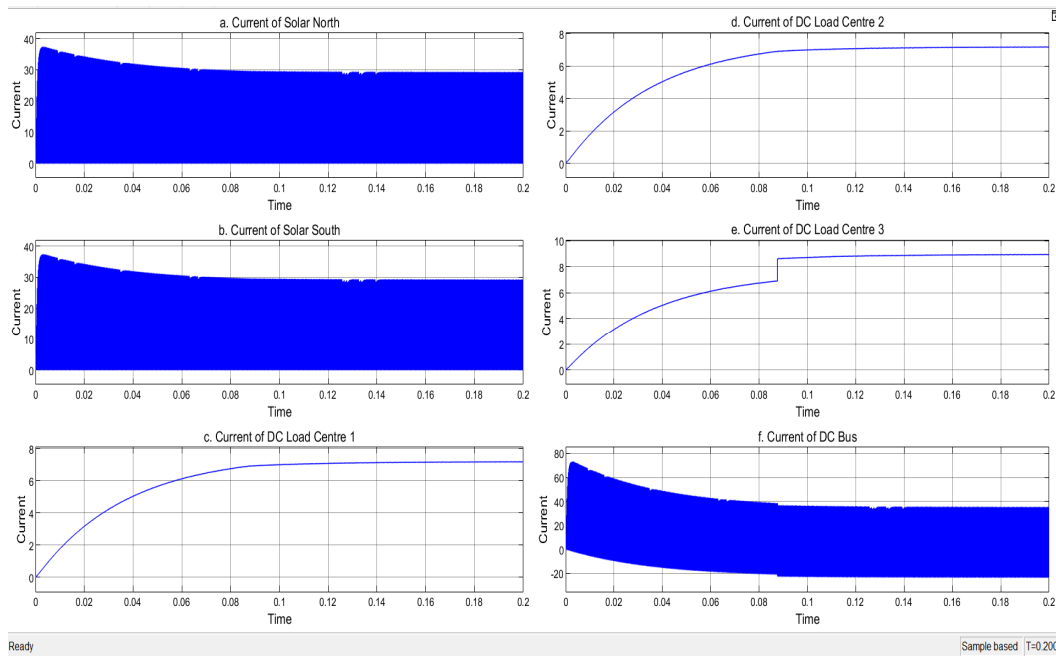


Fig. 13: Current during Pole-to-Pole Fault near the DC Load Centre 3

Fig. 13 represents the current change in various zones when a pole to pole fault is created near the DC load center 3. The DC bus shows a sharp decrease of around 4A when the fault has been created, as shown in Fig. 13.f. the current through the other zones, ie solar north, solar south, DC load center 1 and DC load center 2 as represented in Fig. 13.a., Fig. 13.b., Fig. 13.c., Fig. 13.d., respectively show no significant change. Fig. 13.e., shows a sudden current change when the fault is created in the same zone.

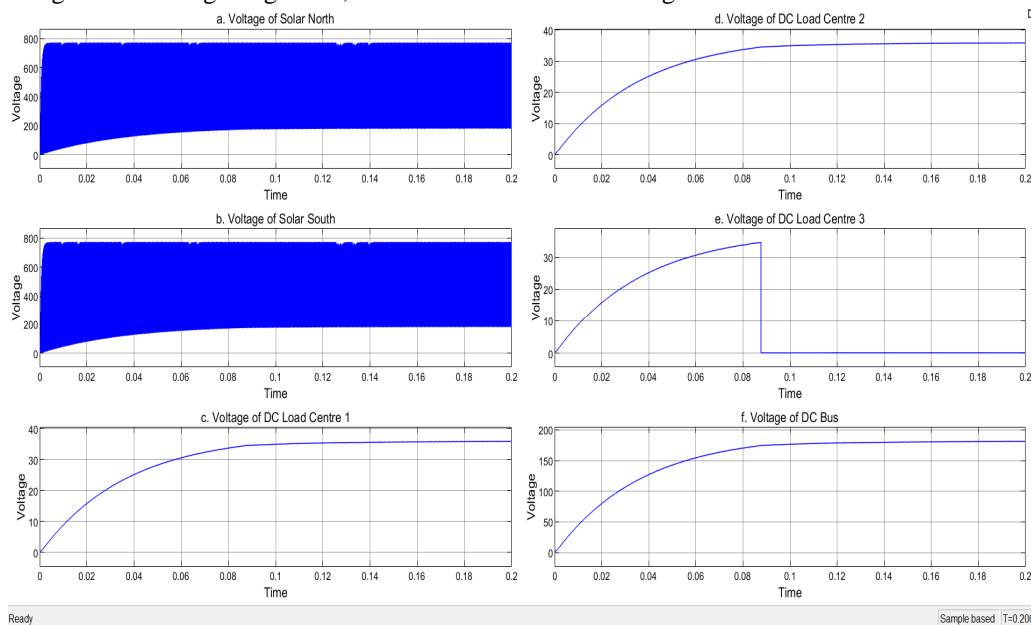


Fig. 14: Voltage during Pole-to-Pole fault near the DC Load Centre 3

Fig. 14 represents the voltage of the system when a pole to pole fault is created near the DC load center 3. While the faulted center shows a sharp voltage drop from steady state value of around 33V to 0V, as shown in Fig. 14.e. the zones of solar north, solar south, DC load center 1, DC load center 2 represented by Fig. 14.a., Fig. 14.b., Fig. 14.c., and Fig. 14.e. respectively show no significant change. The DC bus remains largely unaffected too, as per Fig. 14.f.

G. Fault near the DC Bus

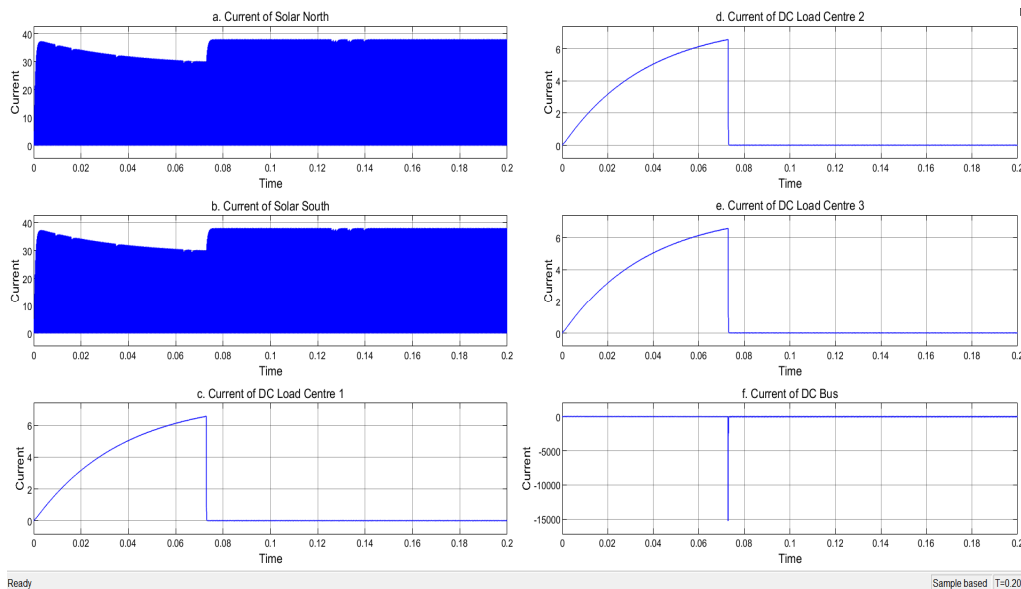


Fig. 15: Current during a Pole-to-Pole Fault near the DC Bus

Fig. 15 represents the current change in the system when a pole-to-pole fault is created near the DC bus. Fig. 15.a. and Fig. 15.b. representing the current of the solar north and the solar south zone respectively shown an increase in the transients by around 10A. the load currents, Fig. 15.c. Fig. 15.d., and Fig. 15.e., representing Load Centre 1, Load Centre 2, and Load Centre 3, show a sharp decline from steady state value to 0A. the current of the faulted zone, in Fig. 15.f., is the most affected, with a momentary decrease to around -15000A.

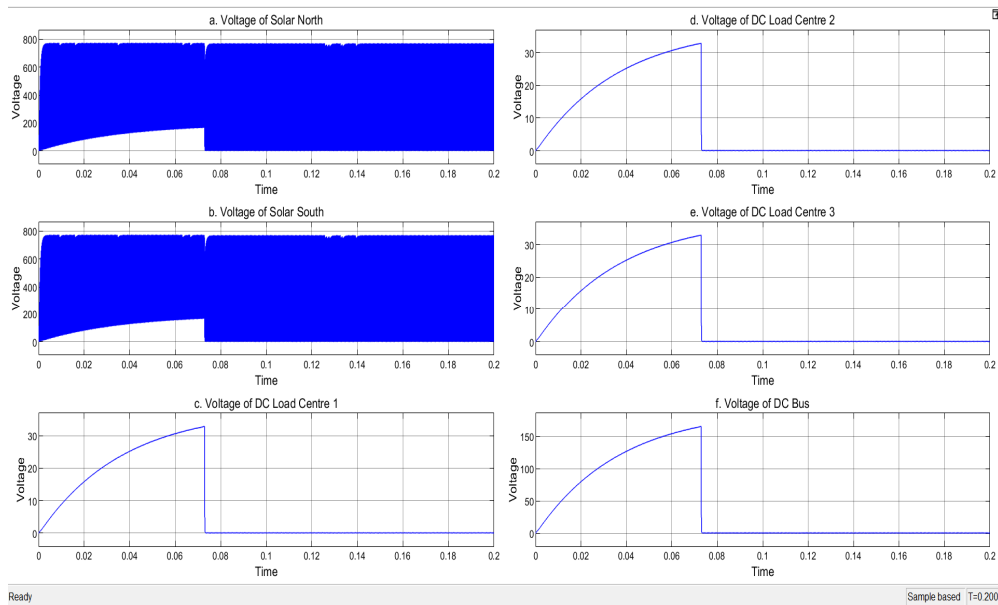


Fig. 16: Voltage during a Pole-to-Pole Fault near the DC Bus

The voltage of various zones when a fault occurs in the common DC bus is presented in Fig. 16. Fig. 16.a. and Fig. 16.b. represent the voltages in the solar north and solar south zone, both of which show a decrease in transients. The Load Centre voltage waveforms, represented by Fig. 16.c., Fig. 16.d., and Fig. 16.e. for Load Centre 1, Load Centre 2, and Load Centre 3 respectively show a fall of voltage from steady state value to 0V. a similar behaviour is observed in the voltage of the DC bus, represented by Fig. 16.f., where a sharp fall is observed when the pole-to-pole fault is created.

IV. PROPOSED ALGORITHM FOR THE DETECTION OF POLE-TO-POLE FAULTS

This section presents the proposed algorithm for the detection of pole-to-pole faults. The work of this algorithm is on the DC Side. The principle of this algorithm is comparing the present current of a zone with the current of the same zone 100 samples ago. The sample time of this system is 1×10^{-5} seconds. Fig. 17. displays the flowchart of the algorithm proposed.

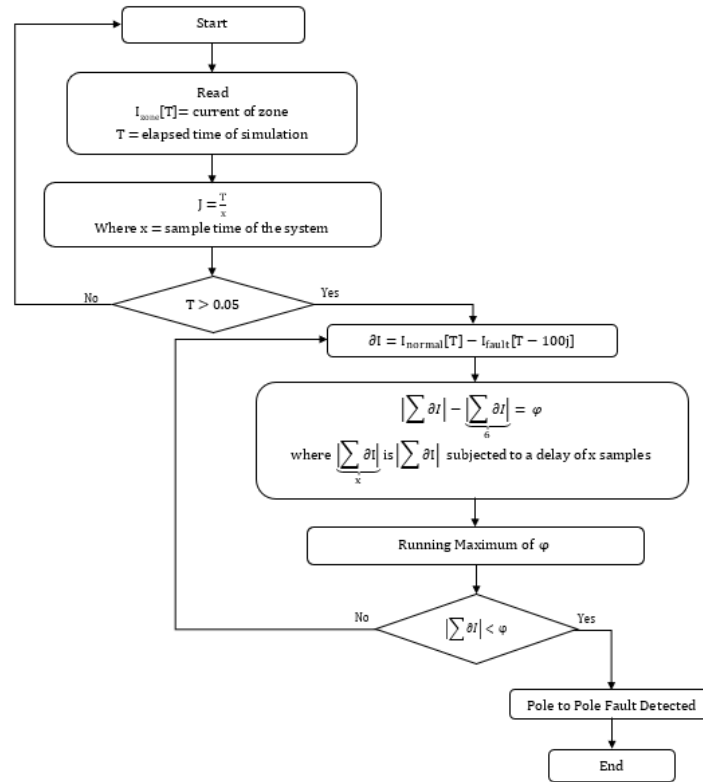


Fig. 17: Flowchart of the Algorithm Proposed

One of the prominent indicators observed in the system when a disturbance (fault) has been created is the rapid change in current. Through the fault analysis, it is observed that pole to pole faults can be detected using change in current. In conventional systems

$$I_{\text{normal}} \ll I_{\text{fault}}$$

However, for the studied system, the above equation does not hold true. This could be attributed to bidirectional flow of power in the microgrid.

$$\Delta I = I_{\text{normal}} - I_{\text{fault}}$$

$$|\Delta I| > 0$$

The constraint with the above observation is that small current changes will be detected as a fault. Thus, the index should be appropriately decided, to avoid false detection of faults. Through trial and error, it was observed that if $j =$ sample time of the system = 10×10^{-5} s and $I_x[t]$ is the current of zone x at a sample t .

$$\partial I = I_{\text{normal}}[t] - I_{\text{fault}}[t - 100j]$$

$$\left| \sum \partial I \right| - \left| \sum \partial I \right| = \varphi$$

where $\left| \sum_x \partial I \right|$ is $\left| \sum \partial I \right|$ subjected to a delay of x samples

The running maximum of φ is always greater than $|\sum \partial I|$ during a fault. Thus, when the running maximum of φ is greater than $|\sum \partial I|$, the controller identifies a pole-to-pole fault.

V. RESULTS AND ANALYSIS

This section of the paper discusses the results when the algorithm is applied to the system under consideration.

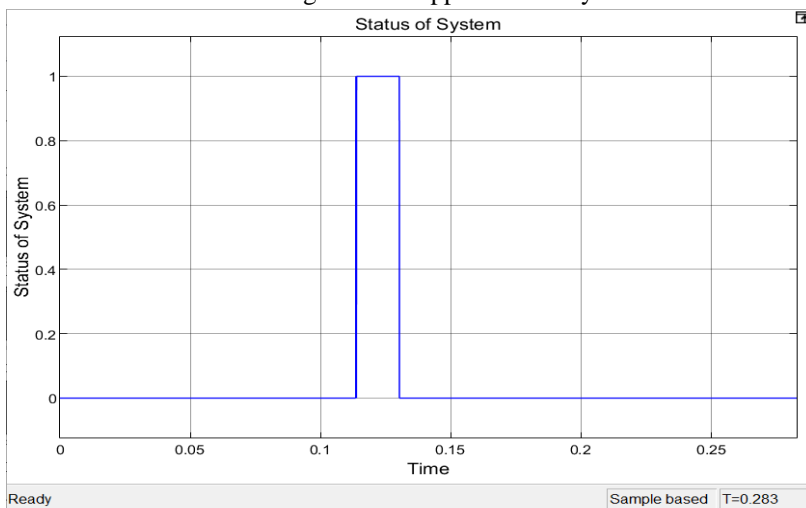


Fig. 18: Output of the Controller when the Algorithm is Applied to the Selected System

The fault is created in the Solar North Zone at a time of 0.115s and the controller output is displayed in Fig. 18. In Fig. 18, 0 represents normal conditions of operation and 1 represents abnormal or faulty conditions of the microgrid. A fault is crated at 0.115s of simulation time.

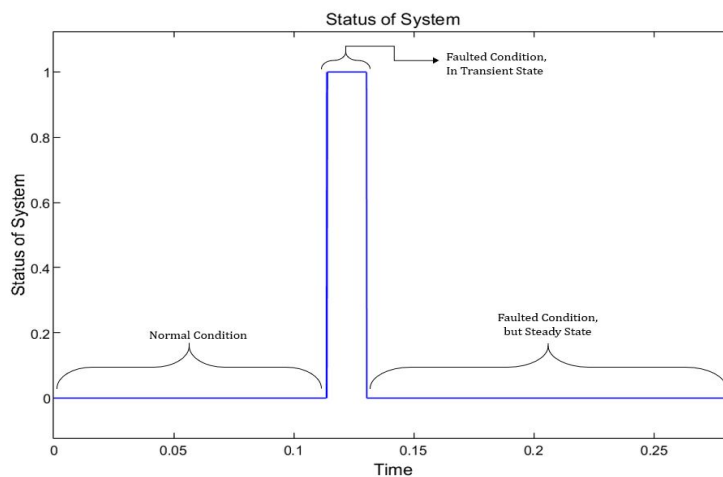


Fig. 19: Analysis of the Controller Output

The analysis of the controller output is graphically presented in Fig. 19. While the detection block represents an output of 1, the system shows a faulted condition and transient state. While the fault detection block shows an output of 0, the system shows steady state conditions.

As the circuit is simulated on an ideal platform, the time taken for operation of the relay is negligible. The time taken to compute the difference between $I_{zone}[t]$ and the $I_{zone}[t-100j]$ where t signifies the elapsed time of simulation and j signifies the sample time as per the flowchart in figure, $100*j$ seconds. If each step of computation takes the duration of one sample time to complete, the total amount of time taken by the system to complete computation = $5*j$ seconds.

$$\text{Time to detect fault} = 100*j + 5*j = 105*j \text{ seconds}$$

While the algorithm can detect pole to pole faults in the system, it is unable to identify the location of the fault in the system. As it is memory drive, it is adaptive, and regularly updates threshold values of current. However, it is marks rapid current changes due to configuration changes as faults and is unable to detect pole to ground faults.

VI. CONCLUSION AND FUTURE WORK

The algorithm was further verified on a hybrid microgrid with a photovoltaic array, wind turbine system, and a battery. While the algorithm can detect pole to pole faults, it is unable to identify the location of the fault. The algorithm is also unable to identify pole to ground faults. Thus, while the algorithm possesses competent speed and reliability, the sensitivity and selectivity of the algorithm are not par with an ideal protection algorithm.

Future work can be conducted to augment the speed of computation, identify the location of the fault, and identify various types of faults. Work can also be carried out to manage power in the system by optimizing the switching of sources.

REFERENCES

- [1] Nirupama P Srinivas and Sangeeta Modi 2022 ECS Trans. 107 13345
- [2] N. Hatzigiorgiou, H. Asano, R. Iravani and C. Marnay, "Microgrids," in IEEE Power and Energy Magazine, vol. 5, no. 4, pp. 78-94, July-Aug. 2007, doi: 10.1109/MPAE.2007.376583.
- [3] X. Zhou, T. Guo and Y. Ma, "An overview on microgrid technology," 2015 IEEE International Conference on Mechatronics and Automation (ICMA), 2015, pp. 76-81, doi: 10.1109/ICMA.2015.7237460.
- [4] V. K. Garg and S. Sharma, "Overview on Microgrid System," 2018 Fifth International Conference on Parallel, Distributed and Grid Computing (PDGC), 2018, pp. 694-699, doi: 10.1109/PDGC.2018.8745849.
- [5] N. Srinivas and S. Modi, "A Comprehensive Review of Microgrid Challenges and Protection Schemes", SPAST Abs, vol. 1, no. 01, Oct. 2021.
- [6] Jayachandran, M., & Ravi, G. (2017). Energy Procedia, 117, 95–103.
- [7] Pankaj Gupta, Ritu Kandari, Ashwani Kumar, Editor(s): Anuradha Tomar, Ritu Kandari, Advances in Smart Grid Power System, Academic Press, 2021, Pages 1-31, ISBN 9780128243374, <https://doi.org/10.1016/B978-012-824337-4.00001-1>.
- [8] T. K. Abdel-Galil, A. E. B. Abu-Elanien, E. F. El-Saadany, A. Girgis, Y. A. R. Mohamed, M. M. A. Salama, et al., Protection coordination planning with distributed generation, Quasys Engco. Inc., 2007.
- [9] S. M. Mirsaedi, D. W. Said, M. H. Mustafa, M. Habibuddin and K. Ghaffari, "Review and analysis of existing protection strategies for micro-grids", Journal of Electrical Systems, vol. 10, no. 1, pp. 1-10, 2014.
- [10] M. P. Reddy and M. Manimozhi. Journal of Green Engineering, vol. 8, no. 2, pp. 89–124, 2018.
- [11] Shahzad, U. and Asgarpoor, S. (2017) A Comprehensive Review of Protection Schemes for Distributed Generation. Energy and Power Engineering, 9, 430-463. doi: 10.4236/epe.2017.98029
- [12] N. P. Srinivas and S. Modi, "Pole-to-Pole Fault Detection Algorithm Using Energy Slope for Microgrids," 2022 International Conference on Electronics and Renewable Systems (ICEARS), 2022, pp. 288-294, doi: 10.1109/ICEARS53579.2022.9752299.
- [13] Sumanth, Akash Srivastava, Sangeeta Modi, 2020, Fault Analysis and Protection of DC Microgrid, INTERNATIONAL JOURNAL OF ENGINEERING RESEARCH & TECHNOLOGY (IJERT) IETE – 2020 (Volume 8 – Issue 11),
- [14] N. Bayati, A. Hajizadeh and M. Soltani, "Protection in DC microgrids: a comparative review," in IET Smart Grid, vol. 1, no. 3, pp. 66-75, 10 2018.
- [15] "DC networks and the challenges of protection," Think-grid.org. [Online]. Available: <https://www.think-grid.org/dc-networks-and-challenges-protection>. [Accessed: 29-Apr-2022].
- [16] Durgaprasad S., Nagaraja S., Modi S. (2022) HVDC Fault Analysis and Protection Scheme. In: P. S., Prabhu N., K. S. (eds) Advances in Renewable Energy and Electric Vehicles. Lecture Notes in Electrical Engineering, vol 767. Springer, Singapore. https://doi.org/10.1007/978-981-16-1642-6_18
- [17] Kamel, R.M., Chaouachi, A., Nagasaka, K.: 'Comparison the performances of three earthing systems for micro-grid protection during the grid connected mode', Smart Grid Renew. Energy, 2011, 2, (03), p. 206
- [18] Mirsaedi, S., Said, D.M., Mustafa, M.W., et al.: 'Progress and problems in micro-grid protection schemes', Renew. Sustain. Energy Rev., 2014, 37, pp.834–839.
- [19] Augustine, Sijo, Quiroz, Jimmy Edward, Reno, Matthew J., and Brahma, Sukumar. DC Microgrid Protection: Review and Challenges. United States: N. p., 2018. Web. doi:10.2172/1465634.



10.22214/IJRASET



45.98



IMPACT FACTOR:
7.129



IMPACT FACTOR:
7.429



INTERNATIONAL JOURNAL FOR RESEARCH

IN APPLIED SCIENCE & ENGINEERING TECHNOLOGY

Call : 08813907089  (24*7 Support on Whatsapp)